Recombination activity of nickel, copper, and oxygen atoms segregating at grain boundaries in mono-like silicon crystals

Yutaka Ohno,[1,a)] Kentaro Kutsukake,[1] Momoko Deura,[1] Ichiro Yonenaga,[1] Yasuo Shimizu,[2] Naoki Ebisawa,[2] Koji Inoue,[2] Yasuyoshi Nagai,[2] Hideto Yoshida,[3] and Seiji Takeda[3]
[1]*Institute for Materials Research (IMR), Tohoku University, Katahira 2-1-1, Aoba-ku, Sendai 980-8577, Japan*
[2]*The Oarai Center, IMR, Tohoku University, Oarai, Ibaraki 311-1313, Japan*
[3]*The Institute of Scientific and Industrial Research (ISIR), Osaka University, 8-1 Mihogaoka, Ibaraki, Osaka 567-0047, Japan*

(Received 19 August 2016; accepted 25 September 2016; published online 6 October 2016)

Three-dimensional distribution of impurity atoms was determined at functional Σ5{013} and small-angle grain boundaries (GBs) in as-grown mono-like silicon crystals by atom probe tomography combined with transmission electron microscopy, and it was correlated with the recombination activity of those GBs, C_{GB}, revealed by photoluminescence imaging. Nickel (Ni), copper (Cu), and oxygen atoms preferentially segregated at the GBs on which arrays of dislocations existed, while those atoms scarcely segregated at Σ5{013} GBs free from dislocations. Silicides containing Ni and Cu about 5 nm in size and oxides about 1 nm in size were formed along the dislocation arrays on those GBs. The number of segregating impurity atoms per unit GB area for Ni and that for Cu, N_{Ni} and N_{Cu}, were in a trade-off correlation with that for oxygen, N_O, as a function of C_{GB}, while the sum of those numbers was almost constant irrespective of the GB character, C_{GB}, and the dislocation density on GBs. C_{GB} would be explained as a linear combination of those numbers: C_{GB} (in %) $\sim 400(0.38N_O + N_{Ni} + N_{Cu})$ (in atoms/nm^2). The GB segregation of oxygen atoms would be better for solar cells, rather than that of metal impurities, from a viewpoint of the conversion efficiency of solar cells. *Published by AIP Publishing.* [http://dx.doi.org/10.1063/1.4964440]

Cast-grown silicon (Si) crystals used for solar cells, such as multicrystalline Si (mc-Si) and mono-like Si, are inevitably introduced detrimental impurity atoms, including transition metals and oxygen, during the growth. Those impurities can limit the carrier diffusion length and consequently influence the solar cell performance, depending on their structural condition in the crystals (such as the atomic arrangement and distribution). The cell performance is particularly decreased by transition metals dispersed in a point defect form, and it can be improved via the precipitation of the metals in silicide forms.[1–3] Meanwhile, grain boundaries (GBs) and dislocations decorated with the metal precipitates increase their recombination activity,[4] depending on the size[5] and chemical composition[6] of the precipitates, as well as on the total number of impurity atoms,[7,8] presumably due to stress nearby the precipitates,[5] and they can cause electrical breakdown[9] and shunts.[10] On the other hand, oxygen does not influence the cell performance when it is in the isolated interstitial form, while it decreases the performance via the formation of point defect complexes such as boron dioxides[11] and via the precipitation at GBs and dislocations,[12,13] as well as in grains.[14–16] Also, such oxygen agglomerates act as a source of harmful subsidiary defects such as metal precipitates[17] and dislocations.[18] A comprehensive knowledge of the structural condition and recombination activity of impurity agglomerates is, accordingly, indispensable to produce cost-effective solar cells by optimizing the structural condition of impurity atoms in cast-grown Si.

In this work, we discuss the recombination activity of impurity atoms segregating at GBs in a mono-like Si. Mono-like Si is quasi-single crystalline Si for solar cells produced by multiple Si seeds, and it can enhance the conversion efficiency of solar cells in comparison with the conventional mc-Si, at a low cost close to that of mc-Si.[19] It is also proposed that, the efficiency can be enhanced via the intentional introduction of functional GBs to suppress the propagation of GBs,[20] dislocations and impurities,[21] with artificially arranged Si seeds. However, dislocations are undesirably introduced at the junctions between the seeds, presumably due to thermal shock,[22,23] impurity segregation,[24] and misorientation between the seeds,[25,26] and they act as a source for the development of dislocation cascades and arrays of dislocations (so called small-angle GBs (SAGBs)).[27] Those GBs have serious impacts on the solar cell efficiency,[28–30] via the segregation of impurity atoms. We have therefore determined three dimensional (3D) distribution of impurity atoms at those GBs by atom probe tomography (APT) combined with transmission electron microscopy (TEM), with a low impurity detection limit about 0.005 at. % on a GB plane simultaneously with a high spatial resolution of 0.4 nm,[31] and clarified the correlation between the distribution and the recombination activity of the GBs, revealed by photoluminescence (PL) imaging with a high spatial resolution of 0.6 μm.[32] This APT-based analytical method enables us to evaluate the recombination activity of silicides and oxides with a size as small as 5 nm or less.

Specimens were cut from a mono-like Si(100) wafer ($100 \times 100 \times 0.3$ mm^3 in size), in which Σ5{013} GBs were artificially introduced to suppress multicrystallization.[20] In

a)Electronic mail: yutakaohno@imr.tohoku.ac.jp

addition, SAGBs were generated around the Σ5{013} GBs. The PL contrast of a GB, C_{GB}, related to the recombination activity of the GB, was determined by PL imaging.[32] C_{GB} was defined as $(I_0 - I_{GB})/I_0$, where I_{GB} and I_0 were the PL intensity at the GB and in the background region, respectively. After the measurement, thin foils for TEM and needles for APT with the GB were prepared by focused-ion-beam (FIB) milling.[31] The structural property of the GB was examined by dark-field (DF) TEM and high-angle annular dark-field (HAADF) scanning TEM (with JEOL JEM-2000EX and ARM200F microscopes, respectively). 3D distribution of impurity atoms at the GB, in a rectangular prism of $40 \times 80 \times 80\,nm^3$, was determined with a local electrode atom probe (Ametek, LEAP4000X HR) with the same experimental condition as in the previous report.[33] The location of the GB plane in 3D impurity maps was determined with pole patterns in two-dimensional Si density maps.[31]

In PL images, some segments of Σ5{013} GBs showed no contrast ($C_{GB} \sim 0\%$) while many segments of the GBs were observed as straight dark lines (Figs. 1(a) and 1(b)). HAADF revealed that the former GB segments consist of a zigzag arrangement of the core structure of the edge dislocation with a Burgers vector a/2⟨011⟩ (Fig. 1(c)), that has no gap state inducing PL contrasts.[34] On the contrary, the latter GB segments had a misorientation of about 0.5° with respect to the Σ5{013} coincidence orientation, and they contained GB dislocations arranged at an interval d of about 20 nm (Fig. 1(d)), with the Burgers vector **b** of a/10[013] (Fig. 1(e)). Those results are consistent with the fact that the recombination activity of a Σ5{013} GB would be controlled by the dislocation density on the GB.[35]

At Σ5{013} GBs free from GB dislocations, a small amount of oxygen atoms (0.006 atoms/nm^2 at the GB plane) segregated (Fig. 2(a)), by which the recombination activity was not increased as shown in Fig. 1(b). Other impurities

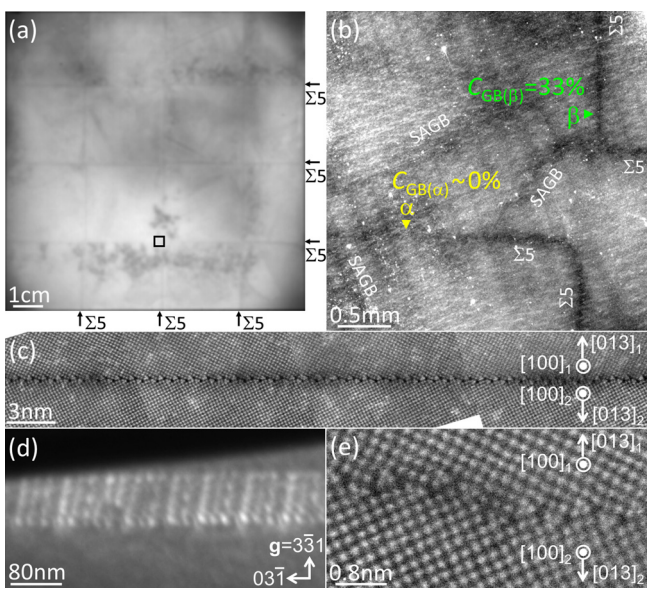

FIG. 1. (a) PL image of a mono-like Si(100) wafer, in which the locations of Σ5{013} GBs are indicated with the arrows. (b) Enlarged PL image of the square area in (a). (c) HAADF image of a Σ5{013} GB at which no PL contrast exhibits, cut from the position α in (b). (d) DF image of a Σ5{013} GB exhibiting PL contrast, cut from the position β in (b). (e) HAADF image of a GB dislocation in (d).

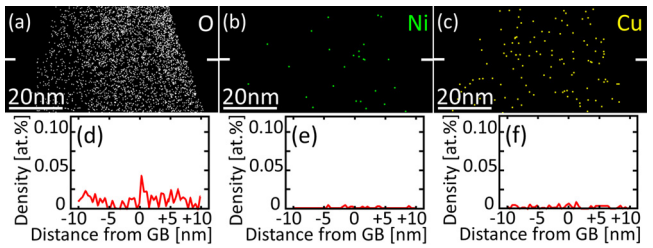

FIG. 2. (a) Projected 3D impurity maps at a perfect Σ5{013} GB cut from the position α in Fig. 1(b); for (a) oxygen, (b) Ni, and (c) Cu atoms, viewed along the GB plane. The solid lines in each figure indicate the GB location. APT density profiles of (d) oxygen, (e) Ni, and (f) Cu atoms across the GB in (a)–(c).

such as Ni (Fig. 2(b)) and Cu (Fig. 2(c)) did not segregate. Thus, the intrinsic segregation ability of Σ5{013} GBs would be small, presumably due to a small GB energy (0.3–0.6 J/m^2),[34,36] like Σ3{111} (~0 J/m^2) and Σ9{221} (~0.3 J/m^2) GBs.[31,37] This suggests that GB dislocations at Σ5{013} GBs should be reduced by minimizing the misorientation at the GBs, to suppress impurity segregation, as well as for potential suppression of the introduction of subsidiary defects,[27] toward high-efficiency solar cells using mono-like Si.

Unlike perfect Σ5{013} GBs, the high density of impurity atoms segregated at Σ5{013} GBs which are decorated with GB dislocations (Fig. 3), similar to the segregation at Σ3{111} GBs decorated with dislocations.[38,39] Oxygen atoms distributed along parallel straight lines arranged at similar intervals (Figs. 3(a) and 3(d)). Also, oxide clusters about 1 nm in size (involving more than three oxygen atoms within a volume of $0.5 \times 0.5 \times 0.5\,nm^3$) were formed on those lines (indicated with the arrowheads in Fig. 3(a)). Such a periodic arrangement was reproduced for another Σ5{013} GB segments with GB dislocations. Considering the morphological similarity between those lines and GB dislocations on the GB, those lines would correspond to the GB dislocations. Nickel (Ni) (Figs. 3(b) and 3(e)) and copper (Cu) (Figs. 3(c) and 3(f)) atoms also segregated on the dislocations. They

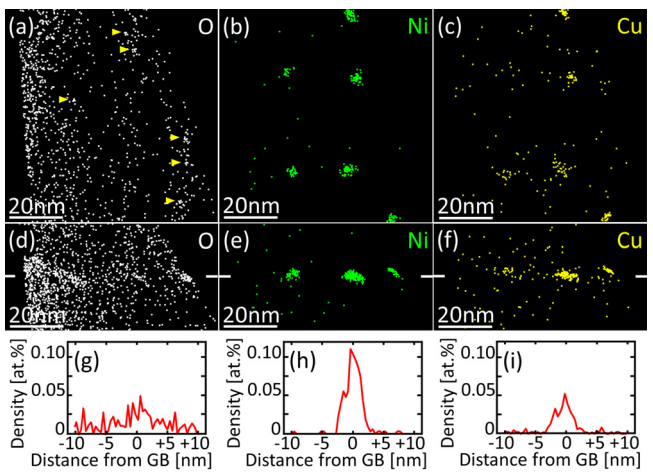

FIG. 3. Projected 3D impurity maps at a Σ5{013} GB with GB dislocations cut from the position β in Fig. 1(b); for ((a), (d)) oxygen, ((b), (e)) Ni, and ((c), (f)) Cu atoms, viewed ((a)–(c)) normal to the GB plane and ((d)–(f)) along the GB dislocations. The solid lines in (d)–(f) indicate the GB location. APT density profiles of (g) oxygen, (h) Ni, and (i) Cu atoms across the GB with GB dislocations in (d)–(f).

rarely existed in an isolated form but formed Ni-rich silicide precipitates containing a partial mole fraction between 10% and 30% of Cu (about 5 nm in size).[40] No another impurity atom was observed at the GBs.

Similar segregation behavior was observed at SAGBs with a high recombination ability. For instance, the GB on nearly (011) shown in Fig. 4(b), with $C_{GB} = 25\%$ (Fig. 4(a)), was an array of parallel dislocations arranged at an interval d of about 15 nm, extending toward [100]. Since the dislocations were invisible with a reflection **g** of $0\bar{2}2$, they were edge-type dislocations with the Burgers vector **b** of a/2[011] (Fig. 4(c)); the GB was a small-angle tilt boundary. Oxygen atoms distributed along the dislocations, and oxide clusters about 1 nm in size and silicide precipitates including Ni and Cu about 5 nm in size were formed on the dislocations (Figs. 4(d)–4(i)).

C_{GB} and 3D impurity distribution were determined for five GB segments involving GB dislocations arranged at different intervals, d. C_{GB} decreased with increasing the misorientation angle at the GBs, $\theta = \tan^{-1}(b/d)$ (Table I), while it increases in impurity-free Si crystals due to the recombination via dislocation levels.[35] Therefore, the recombination activity of dislocations would be small, in comparison with that of impurity atoms. The sum of all impurity atoms segregating at a unit GB area, N_{sum}, was almost constant (0.11–0.13 atoms/nm^2) irrespective of the GB character, C_{GB}, d, and θ (Table I). Meanwhile, the number of segregating impurity atoms per unit GB area for Ni and that for Cu, N_{Ni} and N_{Cu}, increased while that for oxygen, N_O, decreased with increasing C_{GB} (Fig. 5(a)). N_{Ni} and N_{Cu} were, therefore, in a trade-off correlation with N_O as a function of C_{GB}. Thus, C_{GB} would be determined by the number of segregating impurity atoms, rather than by the density of GB dislocations.[35] Because the number of segregating impurity atoms would be in proportion to their recombination activity,[7,8] C_{GB} can be explained as a combination of N_O, N_{Ni}, and N_{Cu}. Under the hypothesis, we can obtain the correlation function: C_{GB} (in %) $\sim 400(0.38N_O + N_{Ni} + N_{Cu})$ (in atoms/nm^2). The constant of proportionality for each impurity should vary depending on the condition during the growth and annealing, since the size[5] and composition[6] of impurity agglomerates can be modified in the condition. Even so, the segregation of oxygen atoms would be better for solar cells, rather than that of metal impurities, from a viewpoint of the conversion efficiency of solar cells.

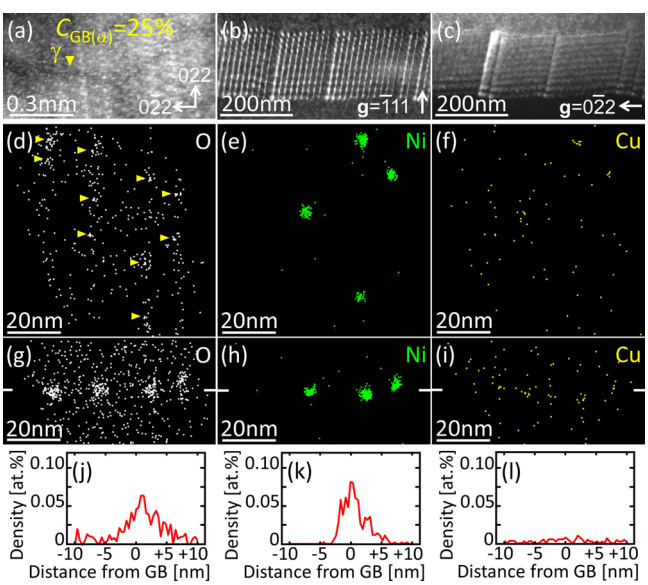

FIG. 4. (a) PL image of a SAGB. ((b), (c)) DF image of the GB on nearly (011) cut from the position γ in (a); taken with **g** of (b) $\bar{1}11$ and (c) $0\bar{2}2$. Projected 3D impurity maps at the GB for ((d), (g)) oxygen, ((e), (h)) Ni, and ((f), (i)) Cu atoms; viewed ((d)–(f)) normal to the GB plane and ((g)–(i)) along the dislocations composing the GB. The solid lines in (g)–(i) indicate the GB location. APT density profiles of (j) oxygen, (k) Ni, and (l) Cu atoms across the GB in (g)–(i).

TABLE I. Characteristics of the GBs involving dislocations examined in the present work.

No.	GB	d[a] (nm)	θ[a] (deg)	C_{GB} (%)	N_{sum} (nm^{-2})
1	Σ5{013}	17–23 (18)	0.4–0.6 (0.5)	33 ± 2	0.11–0.12
2	Σ5{013}	13–20 (16)	0.5–0.8 (0.6)	53 ± 3	0.12–0.15
3	SA{011}	25–26 (26)	0.8–0.9 (0.8)	42 ± 5	0.12–0.13
4	SA{011}	13–20 (14)	1.1–1.7 (1.6)	25 ± 2	0.10–0.12
5	SA{011}	12–13 (13)	1.7–1.8 (1.7)	17 ± 1	0.12

[a]The average value is indicated in the parentheses.

Finally, the segregation behavior of impurity atoms in mono-like Si is discussed. The segregation ability of dislocation arrays for oxygen is examined in Czochralski (CZ)-grown Si crystals, and it is explained in terms of the tensile hydrostatic stress induced by the dislocations.[33] The segregation ability at θ estimated in the CZ crystals is the same order as that in mono-like Si (Fig. 5(a)), suggesting the common segregation mechanism in those crystals. Under the hypothesis, the segregation ability would increase with increasing θ, as observed. Unlike oxygen atoms, most Ni and Cu atoms existed on GBs in silicide forms rather than in isolated forms (Figs. 3 and 4), and the number of silicide precipitates per unit GB area, n_{prec}, decreased with increasing θ (Fig. 5(b)). Precipitation processes of Ni and Cu are examined in detail,[41,42] and an initial process at SAGBs is discussed in terms of a balance between the precipitation and interface energies for the precipitates, and the elastic energy due to lattice mismatch.[43] Silicide precipitates would be formed in Si due to their low precipitation energy, even though they would induce an energy loss due to their interface and elastic energies.[43] n_{prec} might be determined by repulsive elastic interactions between precipitates, and n_{prec} was therefore large for large dislocation intervals.

In conclusion, 3D impurity distribution at GBs in as-grown mono-like Si was examined. Ni, Cu and oxygen atoms preferentially segregated at the GBs on which arrays

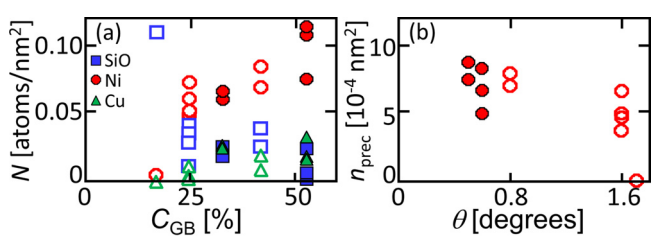

FIG. 5. (a) N_O (square marks), N_{Ni} (circles), and N_{Cu} (triangles) for the GBs involving dislocations as a function of C_{GB}. (b) n_{prec} as a function of θ. The closed and open marks represent the data for Σ5{013} GBs and SAGBs, respectively.

of dislocations existed. Silicides containing Ni and Cu about 5 nm in size and oxides about 1 nm in size were observed along the dislocation arrays, and the recombination activity of the GBs was determined by a linear combination of the numbers of Ni, Cu, and oxygen atoms segregating at the GBs. This nanoscopic finding might provide a guidance to optimize the recombination activity at GBs via the segregation of impurity atoms.

This work was supported by JSPS KAKENHI Grant Nos. 15H03535 (2015-2018) and 15H05413 (2015-2017). HAADF was performed at ISIR under the Cooperative Research Program of Network Joint Research Center for Materials and Devices. APT was performed at the Oarai Center under the Inter-University Cooperative Research Program in IMR.

[1]T. Buonassisi, A. A. Istratov, M. A. Marcus, B. Lai, Z. Cai, S. M. Heald, and E. R. Weber, Nat. Mater. **4**, 676 (2005).
[2]T. Buonassisi, A. A. Istratov, S. Peters, C. Ballif, J. Isenberg, S. Riepe, W. Warta, R. Schindler, G. Willeke, Z. Cai, B. Lai, and E. R. Weber, Appl. Phys. Lett. **87**, 121918 (2005).
[3]M. D. Pickett and T. Buonassisi, Appl. Phys. Lett. **92**, 122103 (2008).
[4]T. Buonassisi, A. A. Istratov, M. D. Pickett, M. Heuer, J. P. Kalejs, G. Hahn, M. A. Marcus, B. Lai, Z. Cai, S. M. Heald, T. F. Ciszek, R. F. Clark, D. W. Cunningham, A. M. Gabor, R. Jonczyk, S. Narayanan, E. Sauar, and E. R. Weber, Prog. Photovoltaics: Res. Appl. **14**, 513 (2006).
[5]P. Gundel, M. C. Schubert, F. D. Heinz, W. Kwapil, W. Warta, G. Martinez-Criado, M. Reiche, and E. R. Weber, J. Appl. Phys. **108**, 103707 (2010).
[6]A. A. Istratov, T. Buonassisi, R. J. McDonald, A. R. Smith, R. Schindler, J. A. Rand, J. P. Kalejs, and E. R. Weber, J. Appl. Phys. **94**, 6552 (2003).
[7]O. F. Vyvenko, T. Buonassisi, A. A. Istratov, E. R. Weber, M. Kittler, and W. Seifert, J. Phys.: Condens. Matter **14**, 13079 (2002).
[8]T. Buonassisi, A. A. Istratov, M. D. Pickett, M. A. Marcus, G. Hahn, S. Riepe, J. Isenberg, W. Warta, G. Willeke, T. F. Ciszek, and E. R. Weber, Appl. Phys. Lett. **87**, 044101 (2005).
[9]W. Kwapil, M. Kasemann, P. Gundel, M. C. Schubert, W. Warta, P. Bronsveld, and G. Coletti, J. Appl. Phys. **106**, 063530 (2009).
[10]T. Buonassisi, O. F. Vyvenko, A. A. Istratov, E. R. Weber, G. Hahn, D. Sontag, J. P. Rakotoniaina, O. Breitenstein, J. Isenberg, and R. Schindler, J. Appl. Phys. **95**, 1556 (2004).
[11]J. Schmidt and K. Bothe, Phys. Rev. B **69**, 024107 (2004).
[12]M. Di Sabatino, S. Binetti, J. Libal, M. Acciarri, H. Nordmark, and E. J. Ovrelid, Sol. Energy Mater. Sol. Cells **95**, 529 (2011).
[13]G. Kato, M. Tajima, F. Okayama, S. Tokumaru, R. Satoda, H. Toyota, and A. Ogura, Acta Phys. Pol., A **125**, 1010 (2014).
[14]J. Haunschild, I. E. Reis, J. Geilker, and S. Rein, Phys. Status Solidi RRL **5**, 199 (2011).
[15]L. Chen, X. Yu, P. Chen, P. Wang, X. Gu, J. Lu, and D. Yang, Sol. Energy Mater. Sol. Cells **95**, 3148 (2011).
[16]J. D. Murphy, R. E. McGuire, K. Bothe, V. V. Voronkov, and R. J. Falster, Sol. Energy Mater. Sol. Cells **120**, 402 (2014).
[17]S. A. McHugo, H. Hieslmair, and E. R. Weber, Appl. Phys. A **64**, 127 (1997).
[18]T. Tachibana, T. Sameshima, T. Kojima, K. Arafune, K. Kakimoto, Y. Miyamura, H. Harada, T. Sekiguchi, Y. Ohshita, and A. Ogura, Jpn. J. Appl. Phys., Part 1 **51**, 02BP08 (2012).
[19]F. Jay, D. Munoz, T. Desrues, E. Pihan, V. Amaral de Oliveira, N. Enjalbert, and A. Jouini, Sol. Energy Mater. Sol. Cells **130**, 690 (2014).
[20]K. Kutsukake, N. Usami, Y. Ohno, Y. Tokumoto, and I. Yonenaga, Appl. Phys. Express **6**, 025505 (2013).
[21]I. Takahashi, S. Joonwichien, T. Iwata, and N. Usami, Appl. Phys. Express **8**, 105501 (2015).
[22]D. Oriwol, E.-R. Carl, A. N. Danilewsky, L. Sylla, W. Seifert, M. Kittler, and H. S. Leipner, Acta Mater. **61**, 6903 (2013).
[23]M. Trempa, C. Reimann, J. Friedrich, G. Muller, A. Krause, L. Sylla, and T. Richter, J. Cryst. Growth **405**, 131 (2014).
[24]M. G. Tsoutsouva, V. A. Oliveira, D. Camel, T. N. TranThi, J. Baruchel, B. Marie, and T. A. Lafford, J. Cryst. Growth **401**, 397 (2014).
[25]M. G. Tsoutsouva, V. A. Oliveira, D. Camel, J. Baruchel, B. Marie, and T. A. Lafford, Acta Mater. **88**, 112 (2015).
[26]M. Trempa, C. Reimann, J. Friedrich, G. Muller, A. Krause, L. Sylla, and T. Richter, Cryst. Res. Technol. **50**, 124 (2015).
[27]B. Ryningen, G. Stokkan, M. Kivambe, T. Ervik, and O. Lohne, Acta Mater. **59**, 7703 (2011).
[28]A. Jouini, D. Ponthenier, H. Lignier, N. Enjalbert, B. Marie, B. Drevet, E. Pihan, C. Cayron, T. Lafford, and D. Camel, Prog. Photovoltaics: Res. Appl. **20**, 735 (2012).
[29]L. Gong, F. Wang, Q. Cai, D. You, and B. Dai, Sol. Energy Mater. Sol. Cells **120**, 289 (2014).
[30]I. Guerrero, V. Parra, T. Carballo, A. Black, M. Miranda, D. Cancillo, B. Moralejo, J. Jimenez, J.-F. Lelievre, and C. Canizo, Prog. Photovoltaics: Res. Appl. **22**, 923 (2014).
[31]Y. Ohno, K. Inoue, Y. Tokumoto, K. Kutsukake, I. Yonenaga, N. Ebisawa, H. Takamizawa, Y. Shimizu, K. Inoue, Y. Nagai, H. Yoshida, and S. Takeda, Appl. Phys. Lett. **103**, 102102 (2013).
[32]K. Kutsukake, M. Deura, Y. Ohno, and I. Yonenaga, Jpn. J. Appl. Phys. **54**, 08KD10 (2015).
[33]Y. Ohno, K. Inoue, K. Fujiwara, M. Deura, K. Kutsukake, I. Yonenaga, Y. Shimizu, K. Inoue, N. Ebisawa, and Y. Nagai, Appl. Phys. Lett. **106**, 251603 (2015).
[34]M. Kohyama, Modell. Simul. Mater. Sci. Eng. **10**, R31 (2002).
[35]K. Kutsukake, N. Usami, K. Fujiwara, Y. Nose, T. Sugawara, T. Shishido, and K. Nakajima, Mater. Trans. **48**, 143 (2007).
[36]V. Yu. Lazebnykh and A. S. Mysovsky, J. Appl. Phys. **118**, 135704 (2015).
[37]T. Kojima, T. Tachibana, N. Kojima, Y. Ohshita, K. Arafune, A. Ogura, and M. Yamaguchi, Jpn. J. Appl. Phys., Part 1 **53**, 04ER20 (2014).
[38]T. Buonassisi, A. A. Istratov, M. D. Pickett, M. A. Marcus, T. F. Ciszek, and E. R. Weber, Appl. Phys. Lett. **89**, 042102 (2006).
[39]Y. Ohno, T. Taishi, Y. Tokumoto, and I. Yonenaga, J. Appl. Phys. **108**, 073514 (2010).
[40]C. Rudolf, P. Saring, L. Stolze, and M. Seibt, Mater. Sci. Eng. B **159–160**, 365 (2009).
[41]M. Seibt, M. Griess, A. A. Istratov, H. Hedemann, A. Sattler, and W. Schroter, Phys. Status Solidi A **166**, 171 (1998).
[42]M. Seibt, H. Hedemann, A. A. Istratov, F. Riedel, A. Sattler, and W. Schroter, Phys. Status Solidi A **171**, 301 (1999).
[43]Y. Ohno, K. Inoue, K. Kutsukake, M. Deura, T. Ohsawa, I. Yonenaga, H. Yoshida, S. Takeda, R. Taniguchi, H. Otsubo, S. R. Nishitani, N. Ebisawa, Y. Shimizu, H. Takamizawa, K. Inoue, and Y. Nagai, Phys. Rev. B **91**, 235315 (2015).